Contents lists available at ScienceDirect

International Communications in Heat and Mass Transfer

A comprehensive study with high-speed camera assisted visualizations of HFO-1234ze(E) condensation inside an enhanced tube

Nima Irannezhad , Luisa Rossetto , Andrea Diani [*]

Department of Industrial Engineering – University of Padua, Italy

ARTICLE INFO

ABSTRACT

Flow condensation of HFO-1234ze(E) inside a helical micro-finned tube of 4.28 mm ID underwent experimentation. Flow patterns were visualized with a high-speed camera while varying vapor qualities from 0.01 to 0.95 and mass fluxes from 100 to 400 kg m^{-2} s^1, at saturation temperature of 30 °C. Intermittent, stratified-wavy, transitional, and annular flow pattern types were identified. The flow pattern map of Doretti et al. (validated by Cavallini et al.) accurately predicted the flow patterns. Heat transfer coefficients (HTCs) and frictional pressure drops (FPDs) were also measured for mass fluxes ranging from 100 to 600 kg m^{-2} s^{-1} at saturation temperatures of 30 °C and 40 °C. Both HTC and FPD elevated with higher mass fluxes and vapor qualities which stemmed from the presence of observed shear stress-driven annular flow patterns. HTC and FPD are generally higher at lower saturation temperatures. Experimental HTC and FPD have been compared against values estimated with empirical models. Furthermore, the average enhancement factor of the micro-finned tube was 2.94 with an area enhancement factor of 2.39. Plotting enhancement factor versus non-dimensional gas velocity provided detailed insight into the augmentation effect of micro-finned tubes under different operating conditions.

1. Introduction

The topic of climate change and its pernicious repercussions and the wariness of the future culminated in the establishment of regulations in various sectors to hinder further exacerbations. The field of refrigeration is not an exception as several regulations are in place. Most of such regulations are designated to decommission refrigerants with high GWP and manage leakages. In the contemporary era, the optimum candidate for the replacement of the current refrigerants with high GWPs is mainly an unresolved aspect. McLinden et al. [1] in their search for the feasibility of adopting new low-GWP refrigerants state that, while no impeccable option exists, HFO-1234yf and HFO-1234ze(E) are among the promising candidates. The possible pivotal rule to be played by HFOs and their mixtures in the future could be overshadowed by the absence of a well-established set of information regarding their performance in comparison to currently used refrigerants and their mixtures. In the attempt to discover possible merits or demerits of HFOs, specifically HFO-1234ze(E), several authors collected experimental information and compared it to that of HFC-134a and other examples that hold a considerable proportion of the market today.

Concerning the heat transfer coefficient inside horizontal smooth tubes, Guo et al. [2] conducted a study of the comparative nature between several refrigerants inside a smooth circular tube of 2 mm as inner diameter (ID). Varying saturation temperatures and mass fluxes between 35 °C and 45 °C and 200 kg m^{-2} s^{-1} and 400 kg m^{-2} s^{-1}, respectively, they concluded that the heat transfer coefficient (HTC) of HFO-1234ze(E) remains the lowest among the tested refrigerants, namely HFC-161, HC-290, HFC-32, HFC-41 and HFC-134a (by 10% compared to HFC-134a). In another attempt with a larger tube size, Longo et al. [3] undertook experimental tests inside a smooth tube of 4 mm ID while varying saturation temperatures between 30 °C and 40 °C and a wide range of mass fluxes. In conclusion, a quite similar set of HTCs under various operating conditions was reported for HFO-1234ze(E), HFC-134a, and HFO-1234yf. Furthermore, a 6 mm ID smooth tube for flow boiling was also under investigation where comparable HTC values were reported for HFO-1234ze(E) and HFC-134a (Grauso et al. [4]). Similar analyses were conducted concerning the pressure drop of HFO-1234ze(E) in smooth tubes. For instance, in the abovementioned paper [4], a slightly higher frictional pressure drop was reported for HFO-1234ze(E) compared to that of HFC-134a. Moreover, Agarwal and Hrnjak [5] experimented on a test section with a close resemblance to [4] in terms

---

Nomenclature

A	surface area, m^2	HC	HydroCarbon
c	specific heat capacity, $J\ kg^{-1}\ K^{-1}$	HFC	HydroFluoroCarbon
EF	enhancement factor	HFO	HydroFluoroOlefin
G	mass flux, $kg\ m^{-2}\ s^{-1}$	HTC	heat transfer coefficient, $W\ m^{-2}\ K^{-1}$
g	gravity, $9.8\ m\ s^{-2}$	ID	inner diameter, m
h	fin height, m; specific enthalpy, $J\ kg^{-1}$	OD	outer diameter, m
i	uncertainty		
J_G^*	critical dimensionless gas velocity	*Greek symbols*	
J_g	dimensionless gas velocity	α	lead angle
M	molar mass, $g\ mol^{-1}$	σ	surface tension, $N\ m^{-1}$
n	number of independent variables	β	helix angle
P	pressure, bar	λ	thermal conductivity, $W\ m^{-1}\ K^{-1}$
S	wall thickness, m	μ	dynamic viscosity, Pa s
T	temperature, °C	ρ	density, $kg\ m^{-3}$
X_{tt}	Martinelli parameter	γ	aspect ratio
x	vapor quality	δ	wall thickness, m
y	general physical quantity		
		Subscript	
Abbreviations		g, v	vapor phase
CLC	calculated	l	liquid phase
EXP	experimental	ref	refrigerant
FPD	frictional pressure drop, Pa	min	minimum
GWP	global warming potential	max	maximum
		test	test section

of tube diameter (6.1 mm ID) and emphasized a large discrepancy as the HFO-1234ze(E) experienced much higher pressure drops compared to HFC-134a. With regard to mini-channels, one can refer to the experimental investigation of Del Col et al. [6] where a 0.96 mm internal diameter channel was tested during condensation and the results demonstrated a higher pressure gradient of HFO-1234ze(E) compared to HFC-134a specifically at higher mass fluxes in which such gradient becomes more pronounced.

Plenty of other authors carried out experimental assessments on HFOs in different test sections which paved the way to a decent grasp of their heat transfer characteristics. Aside from HTC and FPD experimentations, two-phase flow pattern visualization also offers a salient rule in the analysis of two-phase heat transfer as the prevailing flow pattern under certain circumstances will ultimately decide the thermal and hydraulic performances, thus denoting the importance of awareness of the flow patterns. Visualizations of the two-phase flow of HFO-1234ze(E) inside smooth tubes of various diameters are included in the literature (Li and Hrnjak [7], Azzolin et al. [8] and Yang et al. [9]).

As the above examples suggest, information on the heat transfer, pressure losses, and flow patterns of HFO-1234ze(E) inside smooth tubes and various configurations is accruing and will ultimately improve the decisions made regarding the implementation of low-GWP HFO-1234ze(E). This research should also be followed for enhanced surfaces such as micro-finned tubes. Micro-finned tubes offer help in augmenting the heat transfer performance, however, their disadvantage is increased FPD and undesirable increase in pump power consumption for single-phase flow and reduction of saturation temperature for two-phase flow. Considering the flammability rating of HFO-1234ze(E) (A2L [10]), reducing the size of the heat exchanger serves multiple purposes, as it minimizes the refrigerant charge, resulting in both economic and safety benefits. The above statements suggest the need to conduct an experimental investigation on the two-phase heat transfer of HFO-1234ze(E) inside small-diameter micro-finned tubes. A cursory reading of the literature, albeit limited, reveals studies focusing on pressure drop and heat transfer characteristics. Diani et al. [11], having a test section of a 3.4 mm ID (at fin-tip) micro-finned tube, concluded that the HTC of HFO-1234ze(E) closely follows the values of HFC-134a at different mass

fluxes, whereas its FPD are quite larger. Lucchini et al. [12] in their experimental campaign tested HFO-1234ze(E) in a micro-finned tube of 8.96 mm ID (from fin root) during boiling and matched the results to those of HFC-134a. The results illustrated a similar pressure drop at low mass velocities but a more substantial increase (10%) for HFO-1234ze (E) at the mass flux of 220 kg m^{-2} s^{-1} which was hypothesized to stem from larger vapor dynamic viscosity and higher mean velocity of HFO-1234ze(E) at same mass flux. The two fluids showed similar HTCs due to their close liquid thermophysical properties. Another research [13] was centered on condensation inside a micro-finned tube of 7 mm OD with three refrigerants, namely, HFO-1234ze(E), and two HFO/HFC mixtures. The mixture HFO/HFC-515B should be particularly highlighted as research interests emerge because of its close resemblance to HFO-1234ze(E), being a mixture of 91.1%/8.9% of HFO-1234ze(E) and HFC-227ea by mass. FPDs of HFO-1234ze(E) and HFO-515B were reported to be identical and higher than those of HFO/HFC-450A. Regarding the HTC, HFO/HFC-450A was found to present the highest values. Moreover, several correlations were tested and Kedzierski and Goncalves [14], Cavallini et al. [15], Diani et al. [11], and Rollman and Spindler [16] models proved to be the most accurate.

The literature is completely lacking in experimental evaluations dedicated to visualizing the two-phase flow patterns of HFO-1234ze(E) inside micro-finned tubes. Knowledge of flow regimes is indispensable as correlations predicting HTCs are often based on the recognition of flow patterns. Therefore, since HFO-1234ze(E) has not been subjected to visualization inside micro-finned tubes, it is necessary to engage in such an experimental campaign to understand whether the flow pattern is comparable to that of the predetermined maps. In this case, two-phase flow of HFO-1234ze(E) inside a horizontal 5 mm OD micro-finned tube under condensation at a saturation temperature of 30 °C will be visualized with the aid of a high-speed camera. The objective of the visualization is twofold, namely assessing the prevailing flow pattern while altering the parameters of vapor quality (from 0.01 to 0.95) and mass flux (from 100 kg m^{-2} s^{-1} to 400 kg m^{-2} s^{-1}) and comparing to the flow pattern map previously developed [17]. HTCs and FPDs of HFO-1234ze(E) are also assessed by the implementation of another test section where saturation temperatures were set to 30 °C and 40 °C. The

mass fluxes and vapor qualities varied from 100 kg m^{-2} s^{-1} to 600 kg m^{-2} s^{-1} and 0.1 to 0.95 respectively. Aside from an analysis delving into the effects of variation of mass fluxes and vapor qualities, the accuracy of selected predictive models are explored. Furthermore, the paper commits to assessing the enhancement of the micro-finned tube to find links between prevailing flow patterns and the performance of the micro-finned tube.

2. Method

2.1. Experimental facility

Fig. 1 portrays a general layout of the testing facility and its components. The pressure of the thermodynamic cycle is adjusted by the air damper and its mass flow rate is set by the variable speed pump. The hot water fed to the evaporator is integrated with an electric heater which keeps the temperature of water at 70 °C. Refrigerant under super-heated conditions is cooled down to its saturation temperature by the pre-condenser whose cold water source is achieved through a chiller. Condensation is further continued inside the test section implementing a thermostatic bath for its water supply. Ultimately, the refrigerant is subcooled and subsequently percolated before it is pumped.

The temperature of the water cycles along with the temperature and pressure of the refrigerant circuit are duly measured. The temperature acquisition within the test section is made possible by means of T-type-thermocouples (accuracy of ±0.05 K), calibrated with a thermo-resistance Pt100. Measurements of the absolute pressure has been made possible with 3 absolute pressure transducers, having an accuracy of ±1950 Pa, whereas the differential pressure sensor presents an accuracy of ±25 Pa. Water volumetric flow rates at the evaporator and pre-condenser are measured by means of magnetic flow-meters with accuracy of ±0.25% of the reading, whereas the one in the test section shows an accuracy of ±0.50% of the reading. Finally, the refrigerant mass flow rate is gained by a Coriolis-effect mass flow meter, presenting an accuracy of ±0.1% of the reading. All the accuracies are listed in Table 1.

The visualization chamber immediately available at the outlet of the test section allows videotaping of the flow patterns by employing a slow-

Table 1
Accuracy of the experimental instruments.

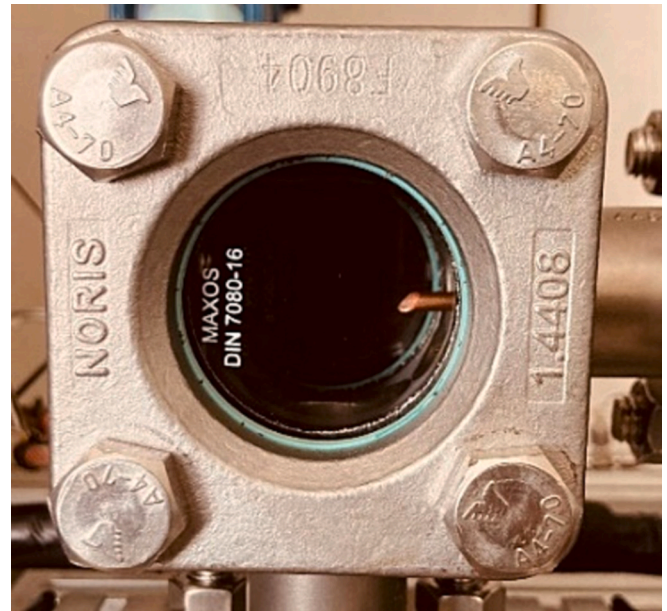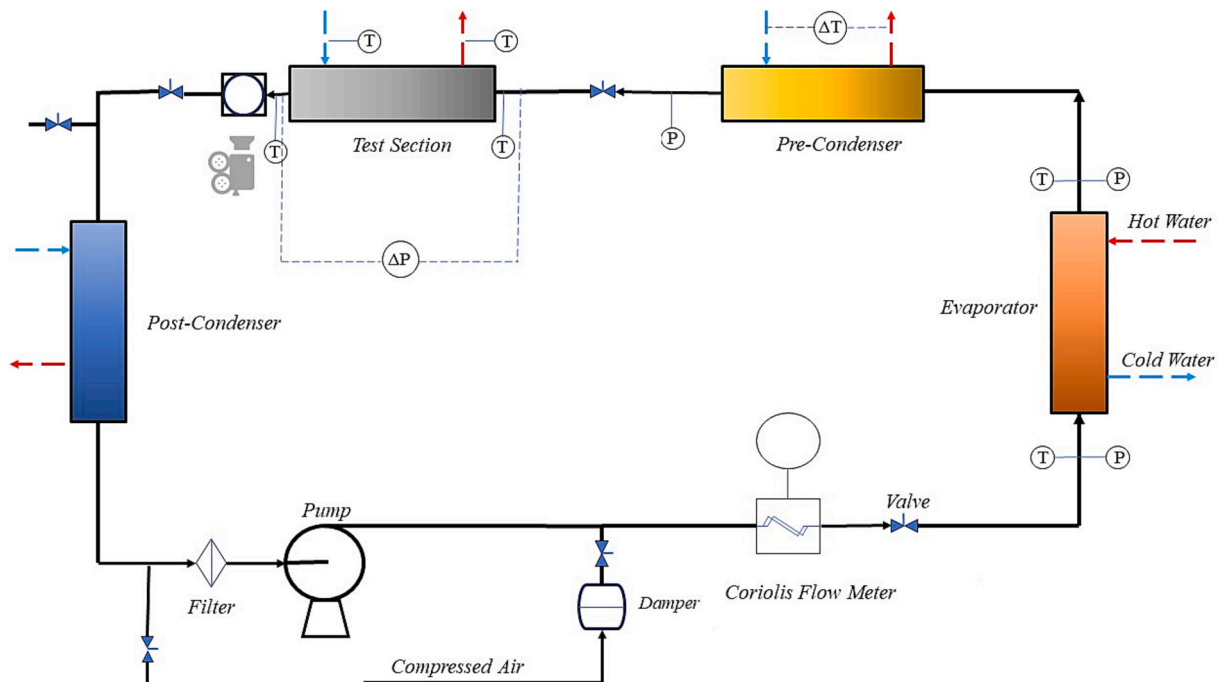|	
T-type thermocouples	±0.05 K
T-type thermopiles	±0.03 K
Coriolis flowmeter	±0.10% of reading
Volumetric flowmeter at pre-condenser	±0.25% of reading
Volumetric flowmeter at evaporator	±0.25% of reading
Volumetric flowmeter at test section	±0.50% of reading
Absolute pressure transducers	±1950 Pa
Differential pressure transducer	±25 Pa

Fig. 2. Visualization chamber.

Fig. 1. Overall schematic of the testing facility.

motion camera. The visualization chamber is present in Fig. 2. As depicted, the micro-finned tube within the chamber is obliquely cut for clear imaging of the exiting flow pattern.

2.2. Test sections

The definition of geometrical parameters in the case of the micro-finned tube under study can be found with the help of Fig. 3. The tube has an outer diameter of 5 mm, 54 fins along the circumference, a lead angle α of 30°, a fin height of 0.15 mm, and a bottom wall thickness of 0.21 mm. The inner diameter, considered at the fin tip, is equal to 4.28 mm. The aspect ratio γ defined as the ratio of fin height and tube diameter at the fin tip is equal to 0.035.

As it can be seen in Fig. 4, the test section is devised to exchange heat with a smooth tube that is helically wrapped around the horizontal micro-finned tube (figure on the left side) and the space between the coils and the micro-finned tube is filled by an alloy melted inside (figure on the right side). Since the study explores both flow patterns and thermal performance during condensation, two slightly different configurations concerning the positioning of thermocouples are chosen.

To perfectly delineate the minor discrepancies between the test sections used for flow pattern and thermal analysis one should refer to Fig. 5 which denotes the placement of T-type thermocouples. For visualization purposes, two T-type thermocouples are planted on the upper and lower sides of the micro-finned tube (red dots in Fig. 5) right after where the heat exchange in the test section concludes. The purpose here is to assist with the verification of observed flow patterns as wall temperature provides preliminary information that can be matched with video analysis of the flow patterns. For thermal performance analysis, six T-type thermocouples (yellow dots in Fig. 5) are placed to capture the average wall temperature of the micro-finned tube that is required for HTC evaluation. It should be noted that the entire test section is insulated with foam to diminish heat losses.

2.3. Data summarization and uncertainty assessment

The HTC and FPD are the thermal and hydraulic parameters considered to assess the behavior of the tested tube. The HTC, based on the energy balance on the water side in the test section, is calculated as:

$$HTC = \frac{\dot{m}_{water,test} \cdot c_{water,test} \cdot \Delta T_{water,test}}{A \left(T_{ref,test,mean} - T_{wall,test,mean} \right)} \quad (1)$$

where A is the equivalent heat transfer area calculated according to a smooth tube and its diameter is selected as the ID of the micro-finned tube at the fin tip. $T_{ref,test,mean}$ is the refrigerant's mean saturation temperature evaluated with the aid of REFPROP10 [18] as a function of the mean pressure. $T_{wall,test,mean}$ is the mean wall temperature of the micro-fin tube. Each experimental HTC is accompanied by the corresponding vapor quality, considered as the average value along the test section. Further details of the data analysis can be read in Diani et al. [13].

Measured values in the abovementioned formulas are assigned with their uncertainties driven by instrumental and random sources. In order to evaluate the uncertainty for the calculated parameter (y) that is the function of independent ones, the method developed by Kline and McClintock [19] is employed. The method to derive the uncertainty of the calculated parameter (i_y) is stated in eq. (2), where x_i denotes the independent variables and i_i their assigned uncertainty.

$$i_y = \sqrt{\sum_{i=1}^{n} \left(\frac{\partial y}{\partial x_i} \bullet i_i \right)^2} \quad (2)$$

The uncertainty for HTC and vapor quality were found and reported in Table 2, split for each saturation temperature.

The pressure gradient is the consequence of the summation of three components, namely gravity, acceleration, and friction pressure gradients. The model of Rouhani and Axelsson [20] has been used to find the void fraction. FPDs can thus be derived. It should be noted that all the parameters are found using REFPROP10 [18] by providing their saturation pressure. When applying the Kline and McKlintock's method [19] neglecting the accuracy on the empirical evaluation of void fraction, the mean, maximum, and minimum uncertainties on the FPD are 0.5%, 1.6%, and 0.1%, respectively. Instead, when considering an accuracy equal to ±0.05 for the void fraction, the mean, maximum, and minimum uncertainties on the FPD are 4.6%, 7.7%, and 0.8%, respectively.

3. Experimental results

3.1. Flow pattern visualization

Fig. 6 depicts the representative flow patterns that were identified after concluding the video analysis. It is pivotal to note that the sequential shots do not possess equal time intervals. In order to have an improved interpretation of pictorial analysis one must refer to the video data set provided. The resolution of the recording camera was set to
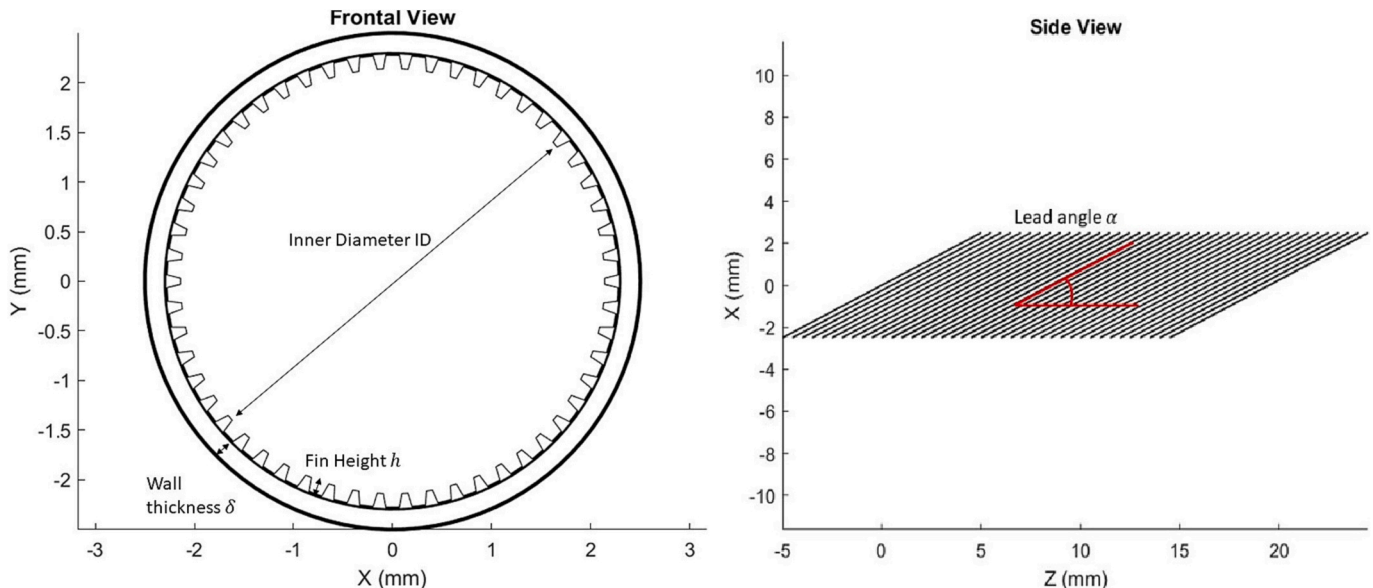

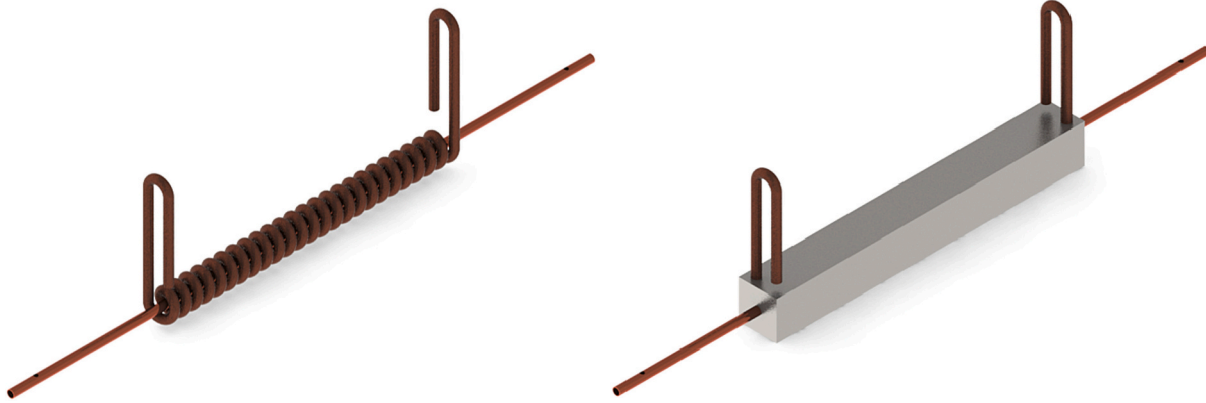**Fig. 3.** Geometrical parameters of the micro-finned tube.
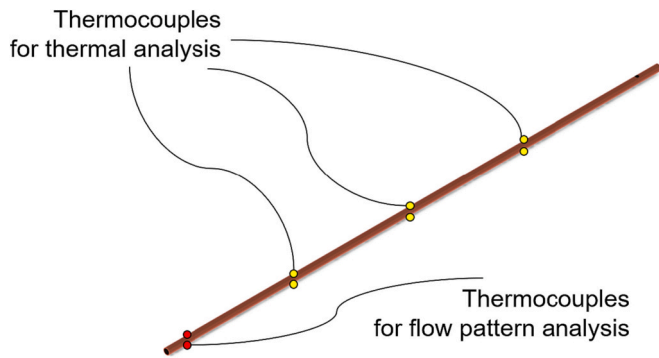
Fig. 4. Overall Schematic of the test section.

Fig. 5. Positioning of the thermocouples in test sections.

Table 2
Uncertainty evaluation.

Uncertainty	30 °C	40 °C
$HTC(i)$ max	±5.4%	±7.4%
$HTC(i)$ mean	±3.7%	±3.0%
$HTC(i)$ min	±2.3%	±2.0%
$x(i)$ max	±0.036	±0.045
$x(i)$ mean	±0.031	±0.031
$x(i)$ min	±0.024	±0.024

1280×720 at 2000 frames per second. Four flow patterns were found and were defined as intermittent, wavy-stratified, annular, and transitional. Overall, 44 videos were recorded for mass fluxes of 100, 150, 200, 300, and 400 kg m^{-2} s^{-1} and vapor qualities from 0.01 to 0.95. Among these 44 videos, 5 videos are available online, and the working conditions of these five videos are summarized in Table 3.

- Intermittent flow pattern: when the waves touch the upper wall, intermittent flow which encompasses slug and plug flow regimes is defined. The name intermittent refers to sporadic contact of the liquid phase with the upper wall among the discrete vapor regions, as it can be grasped from both Fig. 6a and video 1.
- Wavy stratified flow pattern: the wavy-stratified flow is identified when the interface between vapor and liquid phase experiences undulations manifesting in wavy shapes that do not gain enough height to reach the upper side of the tube, as it can be grasped from both Fig. 6b and video 2.
- Transitional flow pattern: the transitional case does not truly represent a flow pattern type and is merely selected to differentiate fully annular flow regimes from semi-developed annular regimes in which the liquid thickness is not strictly evenly distributed along the

circumference (discernable difference of liquid thickness that is higher at the lower bottom of the tube compared to the upper side), as it can be grasped from both Fig. 6c and video 3.
- Annular flow pattern: the fully annular flow regimes possess an identical thickness of the liquid phase along the circumference of the tube, as it can be grasped from both Fig. 6d and videos 4 and 5.

Fig. 7a is constructed to demonstrate the flow patterns as a function of mass flux and vapor quality. In general, the intermittent flow pattern was mostly present at very low vapor qualities. As the mass flux increases, the range of vapor quality in which transitional flow occurs diminishes and the flow pattern immediately switches to an annular type as vapor quality increases. Examples of such are evident at mass fluxes higher than 150 kg m^{-2} s^{-1} in which shear stress dominates and at low vapor qualities (0.3 for 200 kg m^{-2} s^{-1}, 0.2 for 300 kg m^{-2} s^{-1}, and 0.1 for 400 kg m^{-2} s^{-1}) resulting in rapid transition from intermittent to annular flow patterns. The wavy-stratified flow was only present at the lowest mass flux of 100 kg m^{-2} s^{-1} as the shear stress force is not predominant enough to disrupt the surface tension forces present at the interface of the liquid and vapor phase. Aside from visualizations, the upper and lower thermocouples provide insight into the prevailing flow pattern as well. Fig. 7b illustrates the temperature difference between the top and bottom sides of the wall right after the diabatic part of the test section, as a function of mass flux and vapor quality. The aim is to merely assess the fluctuations of temperature between the top and bottom side. As it can be seen, at gravitationally influenced flow patterns of intermittent and wavy-stratified, the wall temperature difference is maximized. At 100 kg m^{-2} s^{-1}, the largest temperature difference is experienced. A similar trend of large temperature difference was reported by Park et al. [21] during wavy-stratified regimes in their experimental campaign. As mass flux increases, the temperature difference reduces until reaching the value of zero, inferring completely identical liquid thickness which results in similar heat transfer performance on both sides of the wall. For temperature differences smaller than 0.4 K, observed flow patterns were either quite close to smooth annular or completely annular flow types where the effect of gravity is non-existent.

Cavallini et al. [15] suggested a new model for the evaluation of HTCs during condensation for pure and azeotropic mixtures inside micro-finned and smooth tubes. The model that was suggested firstly identifies the flow pattern on the basis of whether it is shear stress or gravity-controlled. The process includes the calculation of non-dimensional gas velocity J_g ($J_g = xG/[gD\rho_v(\rho_l - \rho_v)]^{0.5}$) and turbulent-turbulent Martinelli parameter X_{tt} ($X_{tt} = \left(\frac{1-x}{x}\right)^{0.9} \left(\frac{\rho_v}{\rho_l}\right)^{0.5} \left(\frac{\mu_l}{\mu_v}\right)^{0.1}$). Providing two critical non-dimensional gas velocity expressions (J_G^*) for smooth and micro-finned tubes, as a function of X_{tt}, two transition lines from gravitationally controlled regimes to shear stress-controlled
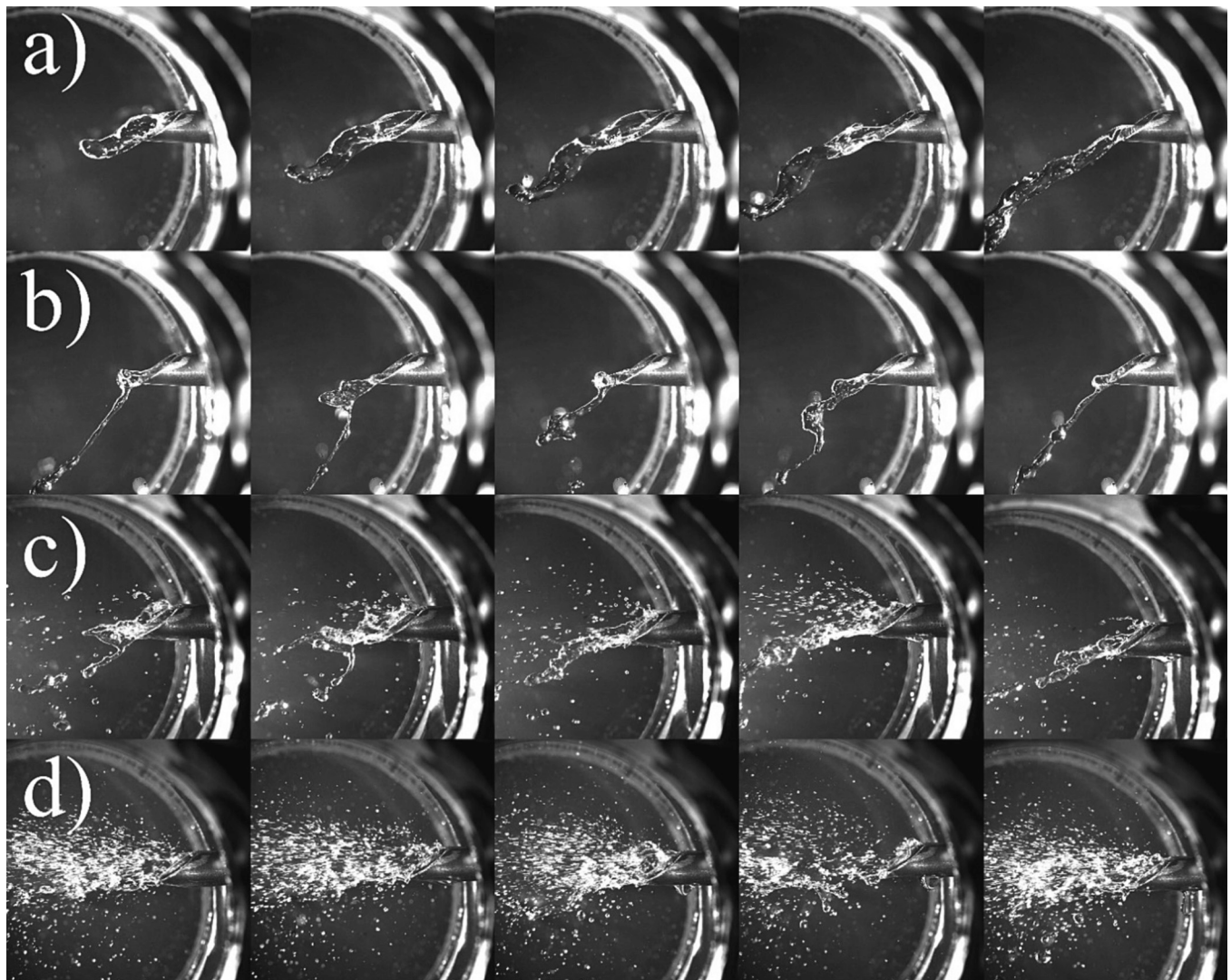
Fig. 6. Photoshoots representing identified flow patterns a) Intermittent flow, b) Wavy-stratified flow, c) Transitional flow, d) Annular flow.

Table 3
Working conditions of the provided videos and photoshoots.

	G [kg m^{-2} s^{-1}]	x [−]
Video #1 and Fig. 6a (intermittent)	100	0.097
Video #2 and Fig. 6b (wavy stratified)	100	0.297
Video #3 and Fig. 6c (transitional)	150	0.406
Video #4 and Fig. 6d (annular)	200	0.512
Video #5 (annular)	300	0.416

regimes are defined.

Fig. 8 is the suggested flow pattern map which was further validated by Doretti et al. [17] with data points and flow patterns of the current research. As mentioned, the map is segregated into two regions: shear stress-controlled and gravity-controlled regimes. Except for annular flow, every other flow pattern identified in the current research experiences at least a degree of ascendency from gravity and is therefore considered gravity-controlled. Although the flow pattern map was not constructed based on results acquired from HFO-type refrigerants, it is in complete consonance with the visualizations. The transitional line suggested for micro-finned tubes provides an excellent prediction for all the mass fluxes.

The congruity between the visualizations and the flow pattern map could stem from close thermophysical properties of HFCs included in the data bank of the research such as HFC-134a to those of HFO-1234ze(E), as it can be verified by using REFPROP10 [18].

3.2. Thermal performance

Fig. 9a-b represents the effect of vapor quality and mass flux on the measured HTC for two different saturation temperatures of 30 °C and 40 °C. By consensus, the HTC augments at higher vapor qualities and mass fluxes. Such augmentation is explicable as elevation in mass flux amplifies the shear stress forces. At high mass fluxes and vapor qualities, the presence of a dominant shear stress force ensures an equal circumferential distribution of the liquid phase which possesses superior thermal properties to that of the vapor phase.

The trend of HTC in the order of increasing vapor quality experiences two anomalies to wit: A. The slope in the lowest mass flux (100 kg m^{-2} s^{-1}) is minimal between the vapor qualities of 0.2 and 0.4 in comparison to other mass fluxes; and B. The growth in the HTC trend suddenly becomes gradual for the case of $G = 600$ kg m^{-2} s^{-1} at vapor quality of x≅0.9 where the HTC is higher for the lower mass flux $G = 400$ kg m^{-2} s^{-1}. The causality for point A is elucidated by referring to flow pattern visualizations as stratification (wavy-stratified flow) was only found at the mass flux of 100 kg m^{-2} s^{-1}. Once stratification takes place, the film thickness becomes minuscule at the top and large at the bottom half of the circumference which heavily impacts the heat transfer performance
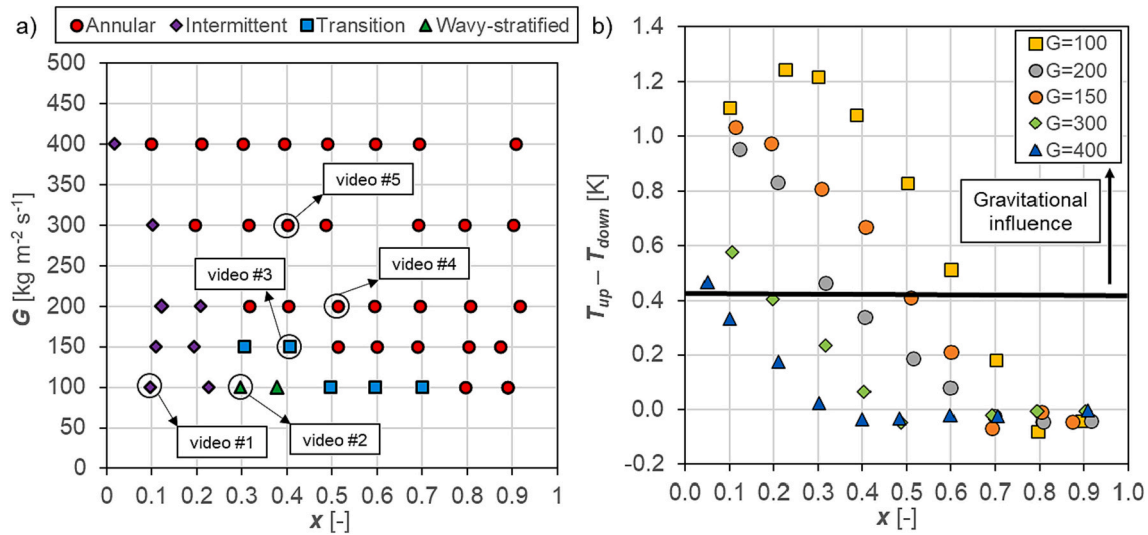
Fig. 7. a) Identified flow patterns on mass flux versus vapor quality b) Subtraction of upper wall temperature from the lower wall as a function of mass flux and vapor quality.
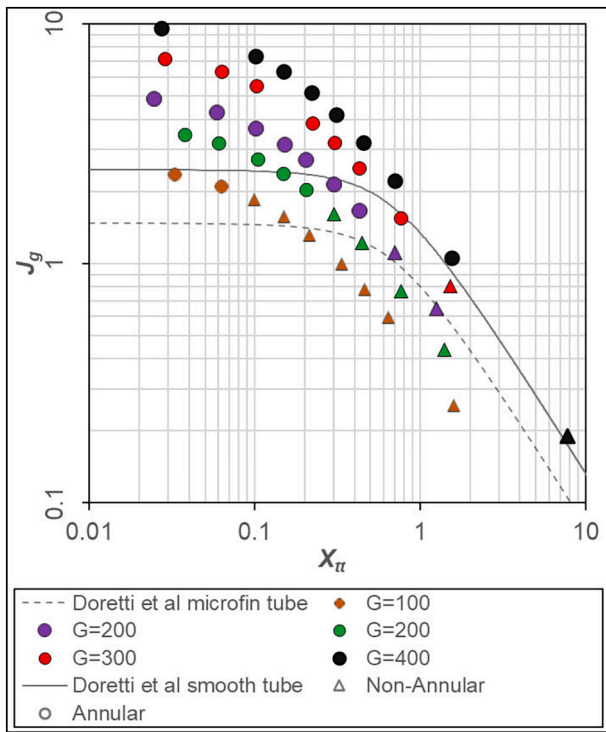

Fig. 8. Flow pattern map by Doretti et al. [17].

and a further increase in vapor quality will not significantly alter it until the flow pattern transmutes into annular type. Point B is particularly important as it infers that an ideal mass flux exists for the micro-finned tube under study. Similar findings to point B have also been reported for helical micro-finned tubes by authors [13,22–24] for helical and by [25] for axially groove tubes, and despite the recorded results, no exact casualties were provided. However, most authors surmised that the unconventional effect lies in the enhancement effect of the micro-finned tube being higher for those of low mass fluxes rather than high mass fluxes such as 600 kg m^{-2} s^{-1}. Regarding the slope with which the HTC increases with vapor quality, having identified the flow patterns, we can offer a compelling argument as to what causes the sudden rapid increase in certain vapor qualities. For instance, at the mass flux of 200 kg m^{-2}

s^{-1} after surpassing the vapor quality of 0.4–0.5, there is an elevation of HTC with a higher slope which stems from the presence of annular flow regimes that were ascertained with visualization that are found in Fig. 7.

The effect of saturation temperature can be better depicted in Fig. 10. Regardless of the mass flux, a saturation temperature of 30 °C possesses HTCs higher than those at 40 °C. The inquiry of what causes the superior HTC for lower saturation temperature is easily answered by considering the thermophysical properties.

Fig. 10 also infers that the heat transfer superiority of the case with 30 °C is mostly pronounced at high vapor qualities for all mass fluxes. The reason for the aforementioned conclusion is also discovered by considering the large discrepancy between the vapor densities and liquid thermal conductivities: a higher saturation temperature implies a higher vapor density (with consequent lower vapor velocity and lower shear stress) as well as a lower liquid thermal conductivity. Similar HTC for both saturation temperatures at low vapor quality was expected as the visualizations demonstrated flow patterns with gravitational influence that ultimately causes the heat transfer characteristics to be mainly dependent on saturation and wall temperature difference rather than vapor thermophysical properties.

Implementing the HTC data acquired, the accuracy of two predictive models is assessed and depicted in Fig. 11. The model of Cavallini et al. [15] had an average absolute deviation of 31.3% and an average relative deviation of 23.7% with overestimations for measured HTC below 10 kW m^{-2} K^{-1}. The model by Kedzierski and Goncalves [14], whose experimental campaign was conducted for condensation of HFCs and near azeotropic mixtures at various saturation temperatures (20°C - 50°C) inside a 9.5 mm OD micro-finned tube with a lead angle of 18°, fin height h of 0.2 mm and wall thickness δ of 0.3 mm, had an average absolute deviation 43.48% and an average relative deviation of 43.44% with the vast majority of data points resulting in overestimation.

3.3. Frictional pressure drop

Fig. 12a-b) shows the measured frictional pressure gradient as a function of mass flux and vapor quality. The general trend of the frictional pressure gradient experiences elevation with increasing vapor quality. The reason for the occurrence should be linked to the observed flow patterns that mostly possess full annular or semi-annular characteristics at high vapor qualities in which vapor velocity is higher. Mass flux also directly upsurges the FPD as it promotes shear stress and velocity which causes higher friction. A noticeable point in Fig. 12 is the FPD reaching a plateau at vapor qualities between 0.7 and 0.8. The
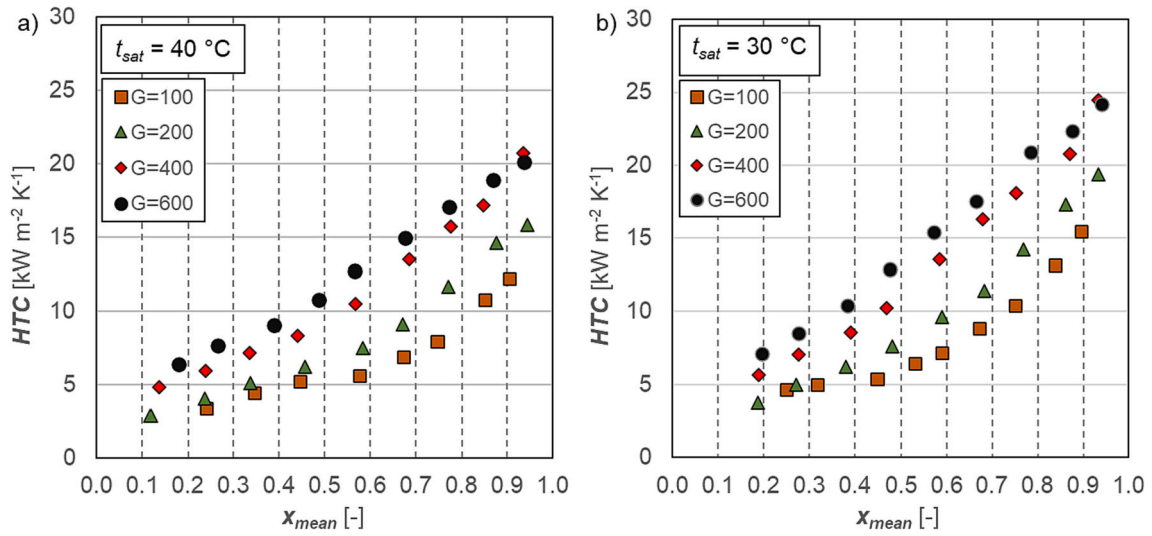
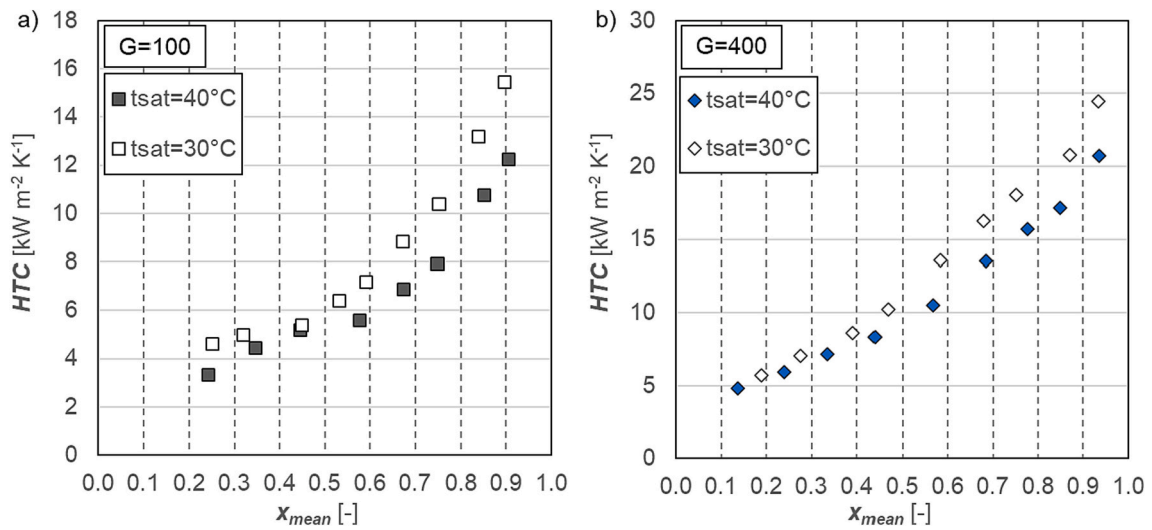**Fig. 9.** Measured HTC versus vapor quality and mass flux for saturation temperature of 40 °C (9a) and 30 °C (9b).

Fig. 10. Effect of saturation temperature on HTC for mass fluxes of a) $G = 100$ kg m^{-2} s^{-1}, b) $G = 400$ kg m^{-2} s^{-1}.
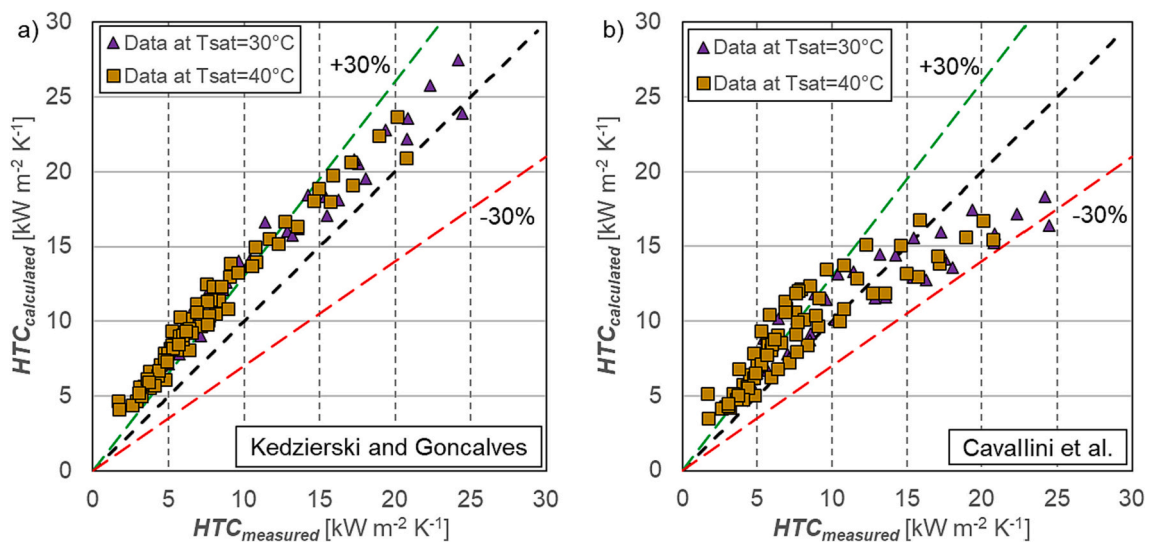

Fig. 11. Calculated values versus experimental results for a) Kedzierski and Goncalves [14] b) Cavallini et al. [15].
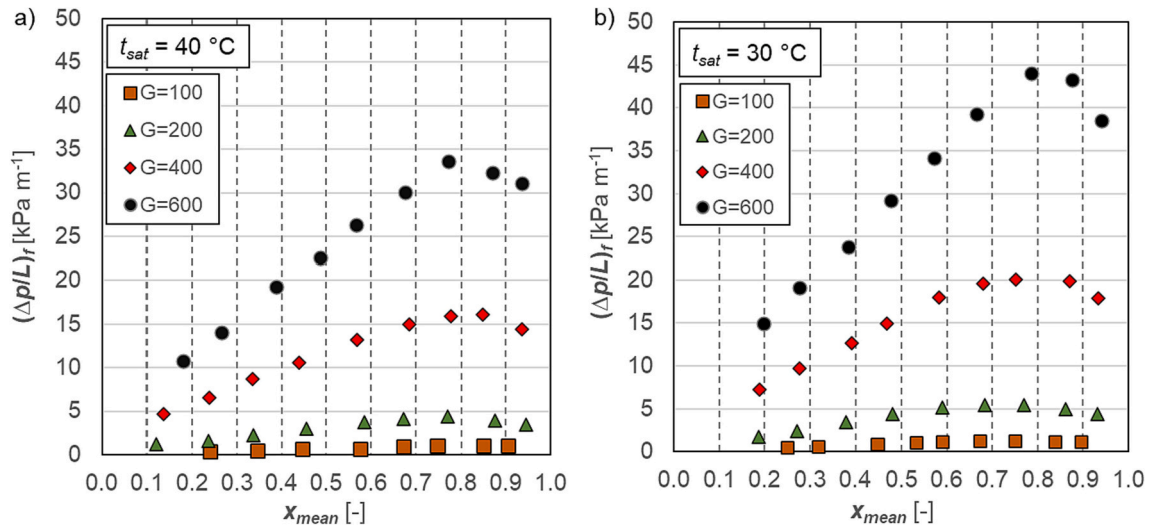
Fig. 12. Measured frictional pressure gradient versus vapor quality and mass flux for saturation temperature of 40 °C (12a) and 30 °C (12b).

reason for such a condition could be related to the entrainment effects at high vapor qualities with the same effect of an increase of the vapor core density.

To demonstrate the effect of saturation temperature in depth Fig. 13 is constructed. At higher saturation pressure, lower frictional pressure gradients were recorded, the reasons for which can be covered by noticing the difference in thermophysical properties such as viscosity and density at different saturation temperature: at a constant mass velocity, a higher saturation temperature leads to a higher vapor density, with consequent lower vapor velocity, and to a lower liquid viscosity. At low values of vapor quality, the difference between measured FPD at two saturation temperatures diminishes as the flow patterns in such conditions are mostly gravitationally influenced, rendering the effect of shear stress and the consequent pressure gradient difference minimal.

The experimental results are also juxtaposed with two predictive models for FPD inside micro-finned tubes. Wu et al. [22], having implemented data from experimental tests on boiling inside five different geometries of the micro-finned tube and collecting data from the literature, stated that their model is applicable to intermittent and annular flow patterns, diameters from 2.1 to 14.8 mm, various refrigerants, mass fluxes from the range of 100 to 650 kg m^{-2} s^{-1} and heat fluxes between 0 and 30 kW m^{-2}. The average relative deviation and the

average absolute deviation were recorded to be −28.9% and 29.4% with underestimations. Diani et al. [11] proposed a model based on validations of experimental measurements on HFO-1234ze(E) inside a 3.4 mm ID micro-finned tube. The model was suggested to be applied for mass fluxes larger than 200 kg m^{-2} s^{-1}. With quite accurate predictions, the average relative deviation and average absolute deviation for their model compared to the current experimental results were recorded to be −10.2% and 14.3% respectively. Fig. 14 demonstrates the calculated values versus the acquired experimental results for both models.

3.4. Efficacy of the micro-finned tube

To assess the performance of micro-finned tubes, several authors conducted experimental research in which HTC of micro-finned tubes was compared to smooth tubes with the same diameter. For such purpose, an expression of enhancement factor was implemented. The enhancement factor (EF) is given as:

$$EF = \frac{HTC_{micro-finned,EXP}}{HTC_{smooth,CLC}} \tag{3}$$

The calculated HTC in the denominator of eq. (3) is obtained by employing the equation of Cavallini et al. [26] developed for smooth
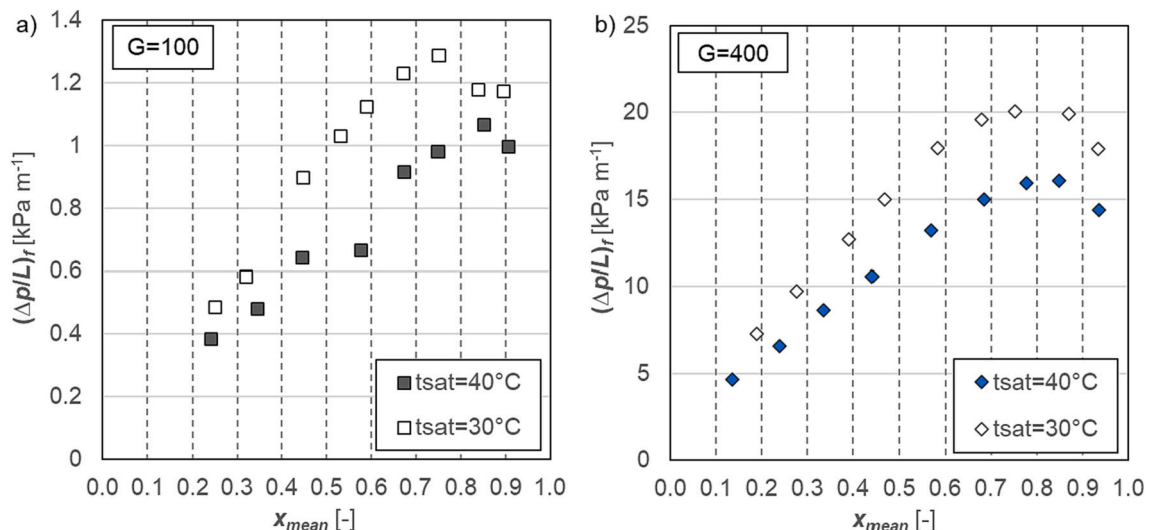

Fig. 13. Effect of saturation temperature on frictional pressure drop for mass fluxes a) $G = 100$ kg m^{-2} s^{-1} b) $G = 400$ kg m^{-2} s^{-1}.
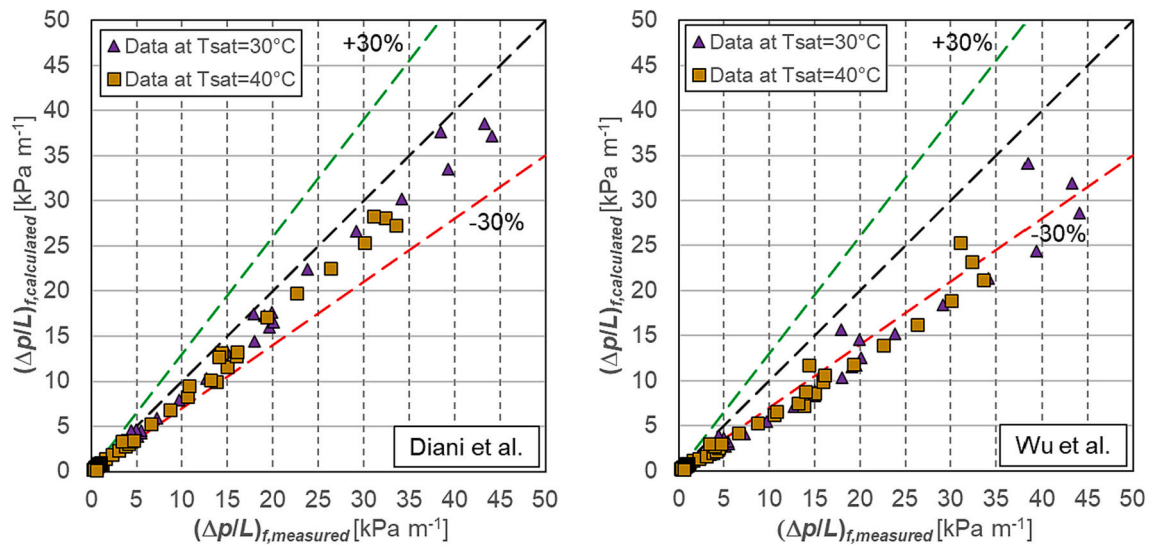
Fig. 14. calculated values versus the experimental results for a) Diani et al. [11] b) Wu et al. [22].

tubes.

Aside from the increase in the heat transfer area, several other aspects were concluded to be the contributors to heat transfer augmentation by micro-finned tubes. Kedzierski and Goncalves [14] referred to liquid-vapor mixing and turbulent mixing near tube walls. Yang and Hrnjack [27] through visualization of helical micro-finned tubes referred to the swirling effect which transports the liquid from the lower side to the upper side of the tube establishing a balanced liquid thickness compared to conventional tubes. Doretti et al. [17] in a comprehensive analysis combined with visualizations of both smooth and helical micro-finned tubes referred to an EF versus vapor quality graph, stating a close correlation between prevailing flow pattern and the effectiveness of micro-finned tubes. In the current research, the conflation of visualization results and a novel graph based on non-dimensional parameters of EF and non-dimensional gas velocity J_g provides a holistic interpretation of how the micro-finned tube performs in various conditions. Considering that the area enhancement factor for the micro-finned tube is approximately equal to the value of 2.39 (evaluated based on the method suggested by Cavallini et al. [15]) Fig. 15 delineates intriguing aspects of the micro-finned tube under study. The micro-finned tube augments thermal performance beyond the sole effect of area enhancement as majority of data points reside beyond the area enhancement line. While efficacy is the result of the joint effect of all contributors, data points are categorized into four areas A, B, C, and D where one effect is more prominent than the others. In area A, even though flow patterns are gravitationally controlled, they still experience better thermal performance than that of smooth tubes under the same condition. Such a result can be directly attributed to the swirling effect of the micro-finned tube under study, enhanced by surface tension, as a suitable choice in lead angle assists the dragging of the liquid phase from the bottom despite the gravitational force that pulls down the liquid during stratified regimes. Regarding area B, the high enhancement factor in annular flow patterns of $G = 100$ kg m^{-2} s^{-1} and $G = 200$ kg m^{-2} s^{-1} is related to the increased turbulence and mixing which resulted in transition to an annular regime at lower values of vapor quality compared to a smooth tube of the same geometry. Fig. 8 in the visualization section testifies to the abovementioned statement as the transition for the smooth tube was predicted to transpire at higher vapor qualities by Doretti et al. [17]. According to the same prediction, at $G = 400$ kg m^{-2} s^{-1}, the smooth and micro-finned tubes are under the same flow regime for the same vapor qualities. However, as it can be seen in area C for the case of $G = 400$ kg m^{-2} s^{-1}, the enhancement factor is improved by a factor larger than the mere area enhancement. Such occurrences can be related to the micro-finned tube's ability to ensure better drainage of the liquid phase at the walls. At area D, for the mass flux of 600 kg m^{-2} s^{-1} and very low vapor quality at 100 kg m^{-2} s^{-1} and 200 kg m^{-2} s^{-1}, the area enhancement is the sole contributor. The reason for the former case could be linked to the fact that at excessively high mass fluxes, the heat transfer surface is less efficient, and the latter case can be related to very low vapor quality which minimizes shear stress forces. It is notable to state the average EF recorded for all mass fluxes that is equal to 2.94. Table 4 reports the enhancement factors for each mass velocity.
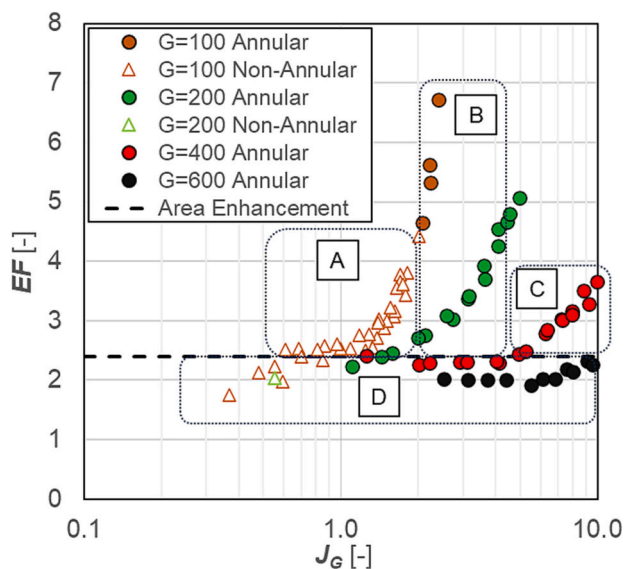

Fig. 15. Enhancement factor versus non-dimensional gas velocity.

Table 4
Average enhancement factors.

G [kg m^{-2} s^{-1}]	EF [−]
100	3.43
200	3.21
400	2.74
600	2.23

4. Conclusions

Mildly flammable low-GWP refrigerant HFO-1234ze(E), a potential alternative for the future of refrigeration, has undergone experimental investigations. For the first time, the condensation flow patterns of HFO-1234ze(E) inside a micro-finned tube of 4.28 mm ID have been visualized by the implementation of a high-speed camera. The recapitulated outcomes are provided as:

1. Four flow patterns of intermittent, wavy-stratified, transitional, and annular were detected. Wavy-stratification only takes place for the lowest mass flux of 100 kg m^{-2} s^{-1} at vapor qualities between 0.3 and 0.4. An intermittent flow pattern is present at low vapor qualities (<0.3). Transitional flow pattern which is defined as the borderline between gravity-influenced and shear stress-influenced flow patterns was only observed for the mass fluxes of 100 kg m^{-2} s^{-1} and 200 kg m^{-2} s^{-1} as for the other mass fluxes of 300 kg m^{-2} s^{-1} and 400 kg m^{-2} s^{-1} the intermittent flow rapidly transmutes to annular flow in the order of increasing vapor quality.

2. The flow pattern map suggested by Doretti et al. [17], designated to predict whether the flow pattern is under the influence of gravity or shear stress, is in complete congruity with the visualized flow patterns in the current research.

3. The heat transfer coefficient is measured to be higher as the mass flux and vapor quality increase and is related to strong shear forces at annular flow patterns. The mass flux of 600 kg m^{-2} s^{-1} experiences lower HTC and higher FPD at a vapor quality of 0.9 compared to that of 400 kg m^{-2} s^{-1} at the same vapor quality. At the mass flux of 100 kg m^{-2} s^{-1} between vapor qualities of 0.3 and 0.4 where stratification was observed, the heat transfer is recorded to have the smallest slope for the trend of HTC as a result of strong gravitational influence. Due to differences in thermophysical properties, saturation temperature of 30 °C had higher HTC and FPD values than 40 °C. Compared to the obtained experimental values, the predictive heat transfer models of Kedzierski and Goncalves [14] and Cavallini et al. [15] had an average relative deviation of 43.4% and 23.7%, respectively.

4. Generally, FPD increases at higher mass flux and vapor qualities due to the presence of an annular flow pattern until an acme is reached and proceeds to reduce at very high vapor qualities ($x > 0.9$). Lower viscosity and lower vapor velocity for a higher saturation temperature of 40 °C result in smaller measured values for FPD compared to 30 °C. Matching the experimental results with the predictive model of Diani et al. [11] resulted in a fairly accurate prediction with an average relative deviation of -10.2%. The model of Wu et al. [22] was also considered where an average relative deviation of -28.9% was obtained.

5. The average enhancement factor for the current micro-finned tube was recorded to be 2.94 with an area enhancement contribution of 2.39. The EF versus non-dimensional gas velocity demonstrated that mass fluxes of 100 kg m^{-2} s^{-1} and 200 kg m^{-2} s^{-1} at medium to high vapor qualities set the highest EF as a result of a quicker transition to an annular flow pattern compared to that of smooth tube. At a mass flux of 600 kg m^{-2} s^{-1}, the enhancement factor is solely from the larger heat transfer area of the micro-finned tube. The same applies to mass fluxes of 100 kg m^{-2} s^{-1} and 200 kg m^{-2} s^{-1} for a very low vapor quality.

Supplementary data to this article can be found online at https://doi.org/10.1016/j.icheatmasstransfer.2023.107203.

CRediT authorship contribution statement

Nima Irannezhad: Data curation, Investigation, Visualization, Writing – original draft. **Luisa Rossetto:** Funding acquisition, Writing – review & editing. **Andrea Diani:** Conceptualization, Investigation, Supervision, Validation, Writing – review & editing.

Declaration of Competing Interest

The authors declare that they have no known competing financial interests or personal relationships that could have appeared to influence the work reported in this paper.

Data availability

Data will be made available on request.

References

[1] M.O. McLinden, A.F. Kazakov, J. Steven Brown, P.A. Domanski, A thermodynamic analysis of refrigerants: possibilities and tradeoffs for low-GWP refrigerants, Int. J. Refrig. 38 (2014) 80–92, https://doi.org/10.1016/j.ijrefrig.2013.09.032.

[2] Q. Guo, M. Li, H. Gu, Condensation heat transfer characteristics of low-GWP refrigerants in a smooth horizontal mini tube, Int. J. Heat Mass Transf. 126 (2018) 26–38, https://doi.org/10.1016/j.ijheatmasstransfer.2018.05.034.

[3] G.A. Longo, S. Mancin, G. Righetti, C. Zilio, Saturated vapour condensation of R134a inside a 4 mm ID horizontal smooth tube: comparison with the low GWP substitutes R152a, R1234yf and R1234ze(E), Int. J. Heat Mass Transf. 133 (2019) 461–473, https://doi.org/10.1016/j.ijheatmasstransfer.2018.12.115.

[4] S. Grauso, R. Mastrullo, A.W. Mauro, J.R. Thome, G.P. Vanoli, Flow pattern map, heat transfer and pressure drops during evaporation of R-1234ze(E) and R134a in a horizontal, circular smooth tube: experiments and assessment of predictive methods, Int. J. Refrig. 36 (2013) 478–491, https://doi.org/10.1016/j.ijrefrig.2012.07.016.

[5] R. Agarwal, P. Hrnjak, Condensation in two phase and desuperheating zone for R1234ze(E), R134a and R32 in horizontal smooth tubes, Int. J. Refrig. 50 (2015) 172–183, https://doi.org/10.1016/j.ijrefrig.2014.10.015.

[6] D. Del Col, M. Bortolato, M. Azzolin, S. Bortolin, Condensation heat transfer and two-phase frictional pressure drop in a single minichannel with R1234ze(E) and other refrigerants, Int. J. Refrig. 50 (2015) 87–103, https://doi.org/10.1016/j.ijrefrig.2014.10.022.

[7] H. Li, P. Hrnjak, Flow visualization of R1234ze(E) in a 0.643 mm microchannel tube, Int. J. Heat Mass Transf. 136 (2019) 950–961, https://doi.org/10.1016/j.ijheatmasstransfer.2019.03.022.

[8] M. Azzolin, A. Berto, S. Bortolin, D. Del Col, Condensation heat transfer of R1234ze(E) and its A1 mixtures in small diameter channels, Int. J. Refrig. 137 (2022) 153–165, https://doi.org/10.1016/j.ijrefrig.2022.02.002.

[9] Z.-Q. Yang, G.-F. Chen, X.-R. Zhuang, Q.-L. Song, Z. Deng, J. Shen, M.-Q. Gong, A new flow pattern map for flow boiling of R1234ze(E) in a horizontal tube, Int. J. Multiphase Flow 98 (2018) 24–35, https://doi.org/10.1016/j.ijmultiphaseflow.2017.08.015.

[10] R. Akasaka, New fundamental equations of state with a common functional form for 2,3,3,3-tetrafluoropropene (R-1234yf) and trans-1,3,3,3-tetrafluoropropene (R-1234ze(E)), Int. J. Thermophys. 32 (2011) 1125–1147, https://doi.org/10.1007/s10765-011-0992-0.

[11] A. Diani, S. Mancin, L. Rossetto, R1234ze(E) flow boiling inside a 3.4 mm ID microfin tube, Int. J. Refrig. 47 (2014) 105–119, https://doi.org/10.1016/j.ijrefrig.2014.07.018.

[12] A. Lucchini, I.M. Carraretto, T.N. Phan, P.G. Pittoni, L.P.M. Colombo, Comparison between R134a and R1234ze(E) during flow boiling in microfin tubes, Fluids. 6 (2021) 417, https://doi.org/10.3390/fluids6110417.

[13] A. Diani, Y. Liu, J. Wen, L. Rossetto, Experimental investigation on the flow condensation of R450A, R515B, and R1234ze(E) in a 7.0 mm OD micro-fin tube, Int. J. Heat Mass Transf. 196 (2022) 123260, https://doi.org/10.1016/j.ijheatmasstransfer.2022.123260.

[14] M.A. Kedzierski, J.M. Goncalves, Horizontal convective condensation of alternative refrigerants within a micro-fin tube, J. Enhanced Heat Transf. 6 (1999) 161–178, https://doi.org/10.1615/JEnhHeatTransf.v6.i2-4.90.

[15] A. Cavallini, D. Del Col, S. Mancin, L. Rossetto, Condensation of pure and near-azeotropic refrigerants in microfin tubes: a new computational procedure, Int. J. Refrig. 32 (2009) 162–174, https://doi.org/10.1016/j.ijrefrig.2008.08.004.

[16] P. Rollmann, K. Spindler, New models for heat transfer and pressure drop during flow boiling of R407C and R410A in a horizontal microfin tube, Int. J. Therm. Sci. 103 (2016) 57–66, https://doi.org/10.1016/j.ijthermalsci.2015.11.010.

[17] L. Doretti, C. Zilio, S. Mancin, A. Cavallini, Condensation flow patterns inside plain and microfin tubes: a review, Int. J. Refrig. 36 (2013) 567–587, https://doi.org/10.1016/j.ijrefrig.2012.10.021.

[18] E.W. Lemmon, M.L. Huber, M.O. McLinden, NIST standard reference database 23, Reference Fluid Thermodynamic and Transport Properties (REFPROP), Version. 9, 2010.

[19] S.J. Kline, Describing uncertainties in single-sample experiments, Mech. Eng. 75 (1963) 3–8. https://cir.nii.ac.jp/crid/1572261549103675008.

[20] S.Z. Rouhani, E. Axelsson, Calculation of void volume fraction in the subcooled and quality boiling regions, Int. J. Heat Mass Transf. 13 (1970) 383–393, https://doi.org/10.1016/0017-9310(70)90114-6.

[21] I. Park, H. Lee, I. Mudawar, Determination of flow regimes and heat transfer coefficient for condensation in horizontal tubes, Int. J. Heat Mass Transf. 80 (2015) 698–716, https://doi.org/10.1016/j.ijheatmasstransfer.2014.09.035.

[22] Z. Wu, Y. Wu, B. Sundén, W. Li, Convective vaporization in micro-fin tubes of different geometries, Exp. Thermal Fluid Sci. 44 (2013) 398–408, https://doi.org/10.1016/j.expthermflusci.2012.07.012.

[23] G.A. Longo, S. Mancin, G. Righetti, C. Zilio, Comparative analysis of microfin vs smooth tubes in R32 and R410A condensation, Int. J. Refrig. 128 (2021) 218–231, https://doi.org/10.1016/j.ijrefrig.2021.04.011.

[24] A. Diani, M. Campanale, L. Rossetto, Experimental study on heat transfer condensation of R1234ze(E) and R134a inside a 4.0 mm OD horizontal microfin tube, Int. J. Heat Mass Transf. 126 (2018) 1316–1325, https://doi.org/10.1016/j.ijheatmasstransfer.2018.06.047.

[25] D. Graham, J.C. Chato, T.A. Newell, Heat transfer and pressure drop during condensation of refrigerant 134a in an axially grooved tube, Int. J. Heat Mass Transf. 42 (1999) 1935–1944, https://doi.org/10.1016/S0017-9310(98)00307-X.

[26] A. Cavallini, G. Censi, D. Del Col, L. Doretti, G.A. Longo, L. Rossetto, Experimental investigation on condensation heat transfer and pressure drop of new HFC refrigerants (R134a, R125, R32, R410A, R236ea) in a horizontal smooth tube, Int. J. Refrig. 24 (2001) 73–87, https://doi.org/10.1016/S0140-7007(00)00070-0.

[27] C.M. Yang, P. Hrnjak, A new flow pattern map for flow boiling of R410A in horizontal micro-fin tubes considering the effect of the helix angle, Int. J. Refrig. 109 (2020) 154–160, https://doi.org/10.1016/j.ijrefrig.2019.09.013.630600793970.